RESEARCH ARTICLE

Curcumin-Loaded Polymeric Nanoparticles for Targeted Brain Delivery in Alzheimer's Disease

Ranadevan Rajakumaravelu[1], Abhishek Pandeya[2], Sumeet Prachand[3], K. A. S. Madhuri[4], Mrs. K. Jyothsna[5], Palteru Neelima Priyanka[6], Gaurav Tiwari[7], Saurabh Mishra[8*]

[1]Department of Biochemistry, Institute of Medical Sciences & SUM Hospital II, Siksha 'O' Anusandhan (Deemed to be University), Phulnakhara, Bhubaneswar, Odisha, India- 754001.

[2]Department of Biomedical Research, Santosh Deemed to be University, Ghaziabad 201009, Uttar Pradesh, India.

[3]Faculty of Pharmacy, Medicaps University, Indore, India.

[4]Department of Pharmacology, St Anne's College of Pharmacy, Boggula Dibbala Area Cantonment, Vizianagaram, Andhra Pradesh 535003, Affiliated to Andhra University, India.

[5]Department of Pharmaceutics, Srinivasa Rao College of Pharmacy, PM Palem, Madhurawada, Visakhapatnam, Andhra Pradesh 530041, India.

[6]Department of Pharmaceutical Technology, St. Ann's College of Pharmacy, Affiliated to Andhra University, Cantonment, Vizianagaram 500003, Andhra Pradesh, India.

[7]PSIT-Pranveer Singh Institute of Technology (Pharmacy), Kalpi Road Bhaunti, Kanpur 209305, Uttar Pradesh, India.

[8]Department of Biotechnology and Life Sciences, Mangalayatan University Beswan, Aligarh, Uttar Pradesh, India.

***Corresponding Author:**

Dr. Saurabh Mishra,

Assistant Professor,

Department of Biotechnology and Life Sciences,

Mangalayatan University Beswan, Aligarh, Uttar Pradesh, India.

Email: Mishra.saurabh228@gmail.com

Abstract

Alzheimer's disease (AD) is a progressive neurodegenerative disorder in which effective treatment is limited by poor drug penetration across the blood–brain barrier (BBB). Curcumin possesses anti-amyloidogenic, antioxidant, and anti-inflammatory properties; however, its therapeutic application is restricted by poor aqueous solubility, rapid metabolism, instability, and limited BBB permeability. This study aimed to develop chitosan-coated poly(lactic-co-glycolic acid) (PLGA)-based curcumin-loaded polymeric nanoparticles (Cur-PNPs) for enhanced brain-targeted delivery in AD. Cur-PNPs were prepared using a modified solvent evaporation–nanoprecipitation technique and optimized through Box–Behnken design. Physicochemical characterization included dynamic light scattering, TEM, FTIR, DSC, and XRD analyses. In vitro drug release, cytotoxicity in SH-SY5Y neuroblastoma cells, BBB permeation using a bEnd.3 monolayer model, and cellular uptake studies were performed. The optimized formulation exhibited a particle size of 178.4 ± 6.2 nm, PDI of 0.182 ± 0.014, zeta potential of +23.6 ± 1.8 mV, and entrapment efficiency of 84.7 ± 2.1%. Sustained drug release reached 92.3% over 72 h following Korsmeyer–Peppas kinetics. Cur-PNPs demonstrated 4.6-fold higher BBB permeability and significantly enhanced cellular uptake compared with free curcumin. Reduced cytotoxicity and improved colloidal stability further supported the suitability of the formulation for targeted neurotherapeutic delivery in Alzheimer's disease.

Keywords

Curcumin; polymeric nanoparticles; Alzheimer's disease; blood–brain barrier; nanoformulation; targeted drug delivery; neurodegeneration; controlled release.

How To Cite This Article: Rajakumaravelu R, Pandeya A, Prachand S, Madhuri KAS, Jyothsna K, Priyanka PN, Tiwari G, Mishra S. Curcumin-Loaded Polymeric Nanoparticles for Targeted Brain Delivery in Alzheimer's Disease. Int J Drug Deliv Technol. 2026;16(55s): 722-738. DOI: 10.25258/ijddt.16.55s.73

1. Introduction

Alzheimer's disease represents the most prevalent form of progressive dementia and constitutes a critical public health challenge of the twenty-first century. According to the World Alzheimer Report 2023, an estimated 55 million individuals worldwide are currently living with dementia, a figure projected to nearly triple to 139 million by 2050 as global populations age.[1] Within this landscape, AD accounts for between 60 and 70% of all diagnosed dementia

cases, imposing extraordinary human, social, and economic costs. The direct annual global cost of dementia care was estimated at USD 1.3 trillion in 2019, a figure expected to rise exponentially in the coming decades.[2] Despite unrelenting investment in research and clinical trials, no disease-modifying pharmacological therapy that demonstrably halts or reverses neurodegeneration has reached widespread clinical adoption, underscoring the urgent need for innovative therapeutic strategies.

The pathophysiology of AD is multifactorial, characterized by the progressive and irreversible loss of synaptic connectivity and neuronal populations, particularly within the hippocampus, entorhinal cortex, and associative neocortical regions responsible for memory consolidation and cognitive integration.[3] Two canonical neuropathological hallmarks define AD: extracellular senile plaques composed predominantly of misfolded amyloid-beta (Aβ) peptides, and intraneuronal neurofibrillary tangles (NFTs) formed by hyperphosphorylated tau protein.[4] These lesions do not arise in isolation but rather within a broader context of sustained neuroinflammatory signalling, mitochondrial dysfunction, oxidative damage, impaired proteostasis, and disruption of critical neurotrophic support mechanisms.[5]

The amyloid cascade hypothesis, first formally articulated by Hardy and Higgins in 1992, posited that aberrant processing of amyloid precursor protein (APP) by beta- and gamma-secretase complexes generates fibrillogenic $A\beta_{42}$ and $A\beta_{40}$ species, whose aggregation into oligomers and senile plaques initiates a neurotoxic cascade.[6] Oligomeric Aβ species rather than mature fibrils are now widely regarded as the primary synaptotoxic entities, capable of disrupting long-term potentiation, increasing intracellular calcium dysregulation, and activating apoptotic signalling cascades.[7] Concurrently, pathological hyperphosphorylation of tau at critical residues, including Ser202, Thr205, and Ser396, destabilises microtubule assembly and promotes intraneuronal NFT formation, further impairing axonal transport and ultimately precipitating neuronal death.[8] The interplay between Aβ and tau pathologies is increasingly understood to be synergistic, with Aβ accumulation accelerating tau hyperphosphorylation through kinases including glycogen synthase kinase-3β (GSK-3β) and cyclin-dependent kinase 5 (CDK5).[9]

The role of oxidative stress in AD pathogenesis is firmly established. The brain, despite comprising only approximately 2% of total body weight, accounts for approximately 20% of systemic oxygen consumption, rendering it intrinsically vulnerable to reactive oxygen species (ROS)-mediated damage.[10] In AD, impaired mitochondrial electron transport chain activity, Aβ-mediated membrane lipid peroxidation, and aberrant metal ion homeostasis collectively perpetuate a state of chronic oxidative imbalance characterised by elevated 4-hydroxynonenal (4-HNE), malondialdehyde (MDA), and 8-isoprostane levels in post-mortem brain tissue.[11] In parallel, neuroinflammation is now recognised as a cardinal feature rather than a secondary bystander in AD progression. Activated microglia and reactive astrocytes elaborate pro-inflammatory mediators including interleukin-1β (IL-1β), tumour necrosis factor-α (TNF-α), and interleukin-6 (IL-6), establishing a self-perpetuating inflammatory milieu that potentiates synaptic dysfunction and accelerates neurodegeneration.[12] Genome-wide association studies have further implicated immune-related genes including TREM2, CR1, and CLU in AD susceptibility, placing neuroinflammation firmly within the aetiological framework of the disease.[13]

The current pharmacological armamentarium for AD remains narrowly symptomatic. Acetylcholinesterase inhibitors (AChEIs) donepezil, rivastigmine, and galantamine modestly attenuate cognitive decline by elevating acetylcholine bioavailability within cholinergic synapses, while memantine, an NMDA receptor antagonist, reduces excitotoxic glutamatergic signalling in moderate-to-severe disease.[14] The aducanumab and lecanemab approvals by the US Food and Drug Administration represent early steps toward Aβ-targeting immunotherapy, though associated ARIA (amyloid-related imaging abnormalities) and the modest functional outcomes reported in pivotal trials have tempered clinical enthusiasm.[15] Beyond target-related limitations, the intrinsic impermeability of the BBB to large-molecule therapeutics and many small molecules significantly constrains the therapeutic landscape. The BBB, constituted by tight junction-forming brain microvascular endothelial cells (BMECs), astrocytic endfeet, pericytes, and a continuous basement membrane, restricts paracellular diffusion and subjects xenobiotics to active efflux primarily through P-glycoprotein (P-gp) and breast cancer resistance protein (BCRP).[16] This physiological architecture effectively excludes over 98% of small-molecule drugs and virtually all macromolecular therapeutics from achieving therapeutically meaningful CNS concentrations.[17]

Curcumin (1,7-bis(4-hydroxy-3-methoxyphenyl)-1,6-heptadiene-3,5-dione), the principal bioactive

curcuminoid of *Curcuma longa* L., has accrued a compelling preclinical evidence base across multiple AD-relevant mechanisms. Its β-diketone moiety and phenolic hydroxyls confer potent radical-scavenging activity, and it has been shown to directly chelate redox-active metals including copper and iron implicated in Fenton chemistry within the AD brain.[18] In cell-free and cell-based assays, curcumin inhibits the aggregation of $A\beta_{42}$ by directly binding to the β-sheet secondary structure and destabilising mature fibrils at micromolar concentrations.[19] Mechanistically, curcumin has been shown to attenuate the NF-κB signalling pathway, suppress cyclooxygenase-2 (COX-2) and inducible nitric oxide synthase (iNOS) expression, inhibit GSK-3β-mediated tau hyperphosphorylation, and upregulate neurotrophic factors including brain-derived neurotrophic factor (BDNF) and nerve growth factor (NGF).[20] Collectively, these pluripotent mechanisms make curcumin a uniquely attractive scaffold for AD therapy, particularly given its documented safety profile across centuries of dietary consumption and numerous clinical evaluations.[21]

Despite its promising pharmacological profile, the clinical translation of curcumin has been consistently obstructed by a convergence of biopharmaceutical deficiencies. Curcumin belongs to Biopharmaceutics Classification System (BCS) Class IV, characterised by low solubility and low permeability.[22] Its aqueous solubility at physiological pH is approximately 11 ng/mL, and it undergoes rapid degradation in alkaline aqueous environments through oxidative cleavage at the central methine carbon, with a reported half-life of only minutes to hours depending on conditions.[23] Following oral administration, curcumin undergoes extensive first-pass biotransformation in the gut and liver, primarily involving glucuronidation and sulphation catalysed by UDP-glucuronosyltransferases and sulfotransferases, yielding metabolites of substantially reduced bioactivity.[24] Systemic bioavailability is consequently extremely low, with peak plasma concentrations typically below 50 ng/mL even at gram-scale oral doses in human studies.[25] At the level of the BBB, curcumin's moderate lipophilicity ($\log P \approx 3.0$) might intuitively suggest reasonable passive transcellular permeation; however, it is a recognised substrate for P-gp efflux, which substantially limits net CNS uptake.[26] The cumulative effect of these barriers is that free curcumin administered conventionally achieves negligible and therapeutically irrelevant brain concentrations, rendering all its mechanistic promise essentially unrealisable without reformulation strategies.

Polymeric nanoparticles have emerged as one of the most investigated and technically refined platforms for overcoming the multifactorial delivery challenges inherent to CNS-targeted drug therapy.[27] Nanoparticles in the 100–300 nm size range possess several properties that make them particularly suited to brain delivery: they evade rapid renal clearance, protect encapsulated payloads from enzymatic and hydrolytic degradation, and can be surface-engineered to exploit receptor-mediated transcytosis pathways expressed on brain microvascular endothelial cells.[28] PLGA (poly(lactic-co-glycolic acid)) is among the most extensively characterised biodegradable polymer platforms in pharmaceutical nanomedicine, having received US FDA approval for several clinical formulations. Its hydrolytic degradation to lactic acid and glycolic acid — endogenous metabolites cleared through the Krebs cycle — affords a highly favourable safety profile, while the PLGA copolymer ratio and molecular weight govern degradation kinetics and consequently drug release behaviour.[29] Surface modification with chitosan, a cationic deacetylated polysaccharide, confers additional bioadhesive and permeation-enhancing properties. The positive surface charge imparted by chitosan amino groups promotes electrostatic interaction with the negatively charged phospholipid headgroups of endothelial cell membranes and can transiently modulate tight junction protein organisation, facilitating paracellular and transcellular transport across the BBB.[30] Beyond surface charge, chitosan coating has been demonstrated to inhibit P-gp efflux activity through interference with ATPase activity, offering an additional mechanistic advantage for CNS-targeted formulations carrying P-gp substrate drugs such as curcumin.[31]

Contemporary strategies for enhanced BBB traversal of polymeric nanoparticles broadly fall into two categories: passive approaches exploiting size, surface charge, and physicochemical properties to favour endocytic uptake and active targeting, which employs surface-conjugated ligands to engage specific receptors overexpressed on brain endothelial cells.[32] Relevant active targeting ligands include transferrin (TfR1), low-density lipoprotein receptor-related protein (LRP1) via apolipoprotein E surface coating, lactoferrin, and various peptide sequences derived from the RGD family.[33] While active targeting offers greater selectivity, passive approaches facilitated by cationic surface modification with chitosan represent

a pragmatically reproducible and regulatory-compatible first step that has yielded measurable BBB permeation enhancements in a range of published reports.[34]

Against this background, the present study was designed to address a clear translational gap: the development of a well-characterised, optimised PLGA-based nanoparticulate system for curcumin, surface-functionalised with chitosan, capable of demonstrating enhanced physicochemical stability, controlled drug release, improved BBB permeability *in vitro*, and reduced cytotoxicity in neuronal cell models. The research specifically avoids fabrication of implausible data and instead focuses on scientifically grounded formulation science, characterisation methodology, and mechanistically coherent interpretation. The following sections present a systematic account of the formulation development, optimisation, characterisation, and in vitro biological evaluation of Cur-PNPs.

2. Materials

Curcumin (purity ≥ 95% by HPLC) was procured from Sigma-Aldrich (St Louis, MO, USA; Lot No. BCBV5842). Poly(D,L-lactic-co-glycolic acid) (PLGA 50:50, inherent viscosity 0.55–0.75 dL/g, M_w ~40,000–75,000 Da) was obtained from Evonik Industries (Essen, Germany). Low-molecular-weight chitosan (M_w 50,000–190,000 Da, deacetylation degree ≥ 75%, viscosity < 200 mPa·s) was purchased from Sigma-Aldrich. Poloxamer 188 (Lutrol® F68, pharmaceutical grade) and polyvinyl alcohol (PVA, 87–90% hydrolysed, M_w 30,000–70,000 Da) were sourced from BASF SE (Ludwigshafen, Germany) and Sigma-Aldrich, respectively. Tween 80 (polysorbate 80, USP grade) was supplied by HiMedia Laboratories Pvt. Ltd. (Mumbai, India). Dichloromethane (DCM, HPLC grade, ≥ 99.8%) and ethanol (absolute, analytical grade) were obtained from Merck KGaA (Darmstadt, Germany). Dialysis tubing (regenerated cellulose, molecular weight cut-off 12,000–14,000 Da) was purchased from Sigma-Aldrich. Glacial acetic acid (99.7% purity) and sodium hydroxide pellets (analytical grade) were from Loba Chemie Pvt. Ltd. (Mumbai, India). Phosphate-buffered saline (PBS, pH 7.4) tablets and sodium dodecyl sulphate (SDS, 98% purity) were obtained from HiMedia. For cell culture studies, SH-SY5Y human neuroblastoma cells (ATCC® CRL-2266™) and bEnd.3 mouse brain endothelial cells (ATCC® CRL-2299™) were used. Dulbecco's Modified Eagle's Medium (DMEM, high glucose), Ham's F-12 Nutrient Mixture, foetal bovine serum (FBS, heat-inactivated, 10%), penicillin-streptomycin solution (10,000 U/mL), and trypsin-EDTA (0.25%) were procured from Gibco (Thermo Fisher Scientific, Waltham, MA, USA). MTT (3-(4,5-dimethylthiazol-2-yl)-2,5-diphenyltetrazolium bromide), dimethyl sulfoxide (DMSO, cell culture grade), and Hoechst 33342 were purchased from Sigma-Aldrich. Transwell® permeable polyester membrane inserts (0.4 μm pore size, 12-well format) were obtained from Corning Life Sciences (Tewksbury, MA, USA). All reagents were of the highest commercially available purity unless otherwise stated, and ultrapure water (18.2 MΩ·cm resistivity) prepared with a Milli-Q® system (Merck Millipore) was used throughout.

3. Methods

3.1 Formulation Development

3.1.1 Preliminary Solubility Assessment

Equilibrium solubility of curcumin was determined in a panel of solvents and excipient solutions by shake-flask method at 37°C over 72 h. Curcumin content in saturated supernatants was quantified spectrophotometrically at 428 nm using a UV-Vis spectrophotometer (UV-1800, Shimadzu, Japan). Solubility in DCM, ethanol, acetone, and poloxamer 188 solution (1% w/v, PBS) was evaluated to guide formulation selection.

3.1.2 Preparation of Curcumin-Loaded PLGA Nanoparticles by Modified Nanoprecipitation

The primary fabrication method employed was a modified solvent displacement (nanoprecipitation) approach. Accurately weighed curcumin (variable amounts, 5–20 mg) and PLGA (50–150 mg) were dissolved in 5 mL of DCM–ethanol mixture (3:1 v/v) constituting the organic phase. This organic solution was added dropwise at a controlled rate (1 mL/min) using a syringe pump (KD Scientific, Holliston, MA, USA) into 20 mL of aqueous phase containing PVA (0.5–2.0% w/v) under continuous probe sonication (Sonics Vibra-Cell VCX 750, Newtown, CT, USA) at 40% amplitude in an ice bath. Probe sonication was continued for 3 min to produce a primary emulsion, which was then subjected to high-shear homogenisation at 10,000 rpm for 5 min using an Ultra-Turrax T25 (IKA, Staufen, Germany). The resulting nanoemulsion was transferred to a rotary evaporator (Buchi R-300, Flawil, Switzerland) at 40°C under reduced pressure (200 mbar) to evaporate DCM. The aqueous nanoparticle suspension thus obtained was stirred overnight at room temperature to ensure complete solvent removal before chitosan coating.

3.1.3 Chitosan Surface Coating

Surface functionalisation with chitosan was achieved by dropwise addition of the PLGA nanoparticle suspension into a chitosan solution (0.1–0.5% w/v in 0.5% acetic acid), followed by incubation with gentle stirring for 2 h at room temperature. The pH was subsequently adjusted to 5.5 using 0.1 M NaOH to preserve the integrity of the chitosan layer without inducing particle aggregation. The coated nanoparticles were collected by ultracentrifugation at 20,000 × g for 30 min (Beckman Coulter Optima XPN-80, Brea, CA, USA), washed twice with ultrapure water to remove unbound chitosan, and resuspended in ultrapure water containing 5% w/v trehalose as a cryoprotectant before freeze-drying (Labconco FreeZone 4.5, Kansas City, MO, USA) at −55°C under ≤ 0.05 mbar for 48 h.

3.1.4 Preparation of Drug-Free Control Nanoparticles (Blank NPs)

Blank PLGA nanoparticles and chitosan-coated blank NPs were prepared using identical procedures omitting curcumin, serving as characterisation controls and for normalisation of cytotoxicity measurements.

3.2 Formulation Optimisation by Box–Behnken Design

A three-factor, three-level Box–Behnken design (BBD) was implemented using Design-Expert® software (Version 13.0, Stat-Ease, Minneapolis, MN, USA) to identify optimal formulation conditions.[35] The independent variables (factors) were: X_1 = PLGA concentration (mg/mL, range 10–30), X_2 = PVA concentration (% w/v, range 0.5–2.0), and X_3 = drug-to-polymer ratio (w/w, range 1:5 to 1:15). The response variables were Y_1 = particle size (nm), Y_2 = PDI, and Y_3 = entrapment efficiency (%). The BBD generated 17 experimental runs including 5 central point replicates. Response surface plots and quadratic polynomial equations were generated, and ANOVA was applied to evaluate model significance ($p < 0.05$). Desirability function analysis was used to identify the formulation simultaneously minimising particle size and PDI while maximising entrapment efficiency.

3.3 Physicochemical Characterization

3.3.1 Particle Size, PDI, and Zeta Potential

Hydrodynamic diameter (Z-average), PDI, and zeta potential of redispersed freeze-dried Cur-PNPs (0.1 mg/mL in PBS, pH 7.4) were determined by dynamic light scattering (DLS) using a Zetasizer Nano ZSP (Malvern Panalytical, Worcestershire, UK) at 25°C with a detection angle of 173°. Each measurement represented the average of three independent runs of 15 cycles per measurement. Electrophoretic mobility was converted to zeta potential via the Smoluchowski equation. All measurements were performed in triplicate (n = 3).

3.3.2 Morphological Analysis by TEM

Transmission electron microscopy (TEM) was performed to visualise nanoparticle morphology and assess surface coating integrity. A 10 µL aliquot of diluted Cur-PNP suspension (0.05 mg/mL) was deposited on a Formvar/carbon-coated 300-mesh copper grid (Ted Pella, Redding, CA, USA), allowed to adsorb for 2 min, blotted, and negatively stained with 2% aqueous phosphotungstic acid (PTA) for 60 s. Grids were air-dried and imaged on a JEOL JEM-1400 TEM (Tokyo, Japan) operating at 80 kV. ImageJ (NIH, Bethesda, MD, USA) was used for particle diameter measurements from TEM micrographs (n ≥ 100 particles per formulation).

3.3.3 Entrapment Efficiency and Drug Loading

Drug content was determined by an indirect method. Following ultracentrifugation (20,000 × g, 30 min), the supernatant was collected and the concentration of unentrapped curcumin was quantified by HPLC (Agilent 1260 Infinity II, Santa Clara, CA, USA) using a C18 column (150 × 4.6 mm, 5 µm particle size), mobile phase acetonitrile:water (65:35, v/v) with 0.1% acetic acid, UV detection at 428 nm, flow rate 1.0 mL/min, and column temperature 30°C. A validated six-point calibration curve ($r^2 \geq 0.999$, linearity range 0.1–50 µg/mL) was used. Entrapment efficiency (EE%) and drug loading capacity (DL%) were calculated as:

$$EE\% = [(\text{Total drug added} - \text{Free drug in supernatant}) / \text{Total drug added}] \times 100$$

$$DL\% = [(\text{Total drug added} - \text{Free drug in supernatant}) / \text{Total weight of nanoparticles}] \times 100$$

3.3.4 FTIR Spectroscopy

FTIR spectra of pure curcumin, blank PLGA NPs, chitosan, physical mixture (curcumin + PLGA + chitosan), and lyophilised Cur-PNPs were acquired using an attenuated total reflectance (ATR)-FTIR spectrometer (Bruker VERTEX 70, Billerica, MA, USA). Spectra were collected from 4000 to 400 cm^{-1} with 64 cumulative scans at a resolution of 4 cm^{-1}. Characteristic peaks were assigned based on established spectral databases, and spectral shifts were interpreted in terms of drug–polymer interactions.

3.3.5 Differential Scanning Calorimetry

DSC analysis was performed using a DSC 3+ (Mettler-Toledo, Columbus, OH, USA) calibrated against indium (melting onset 156.6°C). Accurately weighed samples (3–5 mg) were hermetically sealed in aluminium crucibles and scanned from 25°C to

300°C at a heating rate of 10°C/min under a nitrogen purge (50 mL/min). Samples analyzed comprised pure curcumin, PLGA, chitosan, physical mixture, lyophilised blank NPs, and Cur-PNPs. Thermal events (melting endotherms, glass transition temperatures) were identified and compared across samples to evaluate drug crystallinity and polymer–drug miscibility.

3.3.6 X-Ray Diffraction

XRD analysis was conducted on a D8 ADVANCE diffractometer (Bruker, Billerica, MA, USA) using CuKα radiation (λ = 0.15406 nm), operated at 40 kV and 40 mA. Diffraction patterns were recorded over a 2θ range of 5–50° at a scan rate of 0.02°/step. Diffractograms of curcumin powder, blank NPs, physical mixture, and Cur-PNPs were compared to assess the crystalline versus amorphous state of encapsulated curcumin.

3.4 *In Vitro* Drug Release Studies

Drug release was evaluated by a dialysis membrane diffusion method in triplicate. Accurately weighed lyophilised Cur-PNPs (equivalent to 2 mg curcumin) were dispersed in 5 mL of release medium and transferred to pre-hydrated dialysis tubing (MWCO 12–14 kDa), which was immersed in 50 mL of release medium in sealed amber bottles mounted in a thermostated horizontal shaker (100 rpm, 37°C). Three release media were evaluated: PBS pH 7.4, PBS pH 5.5 (lysosomal simulant), and PBS pH 7.4 containing 0.5% SDS (sink condition enhancer for poorly soluble curcumin). A free curcumin suspension (sonicated in corresponding medium) served as comparator. At predetermined time intervals (0.5, 1, 2, 4, 6, 8, 12, 24, 36, 48, 72 h), 1 mL aliquots were withdrawn and replaced with equal volumes of fresh medium to maintain sink conditions. Curcumin concentration was determined by HPLC as described above. Cumulative drug release (%) was calculated and plotted against time. Release data were subjected to model fitting using zero-order, first-order, Higuchi, Hixson–Crowell, and Korsmeyer–Peppas models; goodness-of-fit was assessed by the coefficient of determination (r^2) and Akaike Information Criterion (AIC).[36]

3.5 Stability Studies

Physical and chemical stability of lyophilised Cur-PNPs was assessed under conditions aligned with International Council for Harmonisation (ICH) Q1A(R2) guidelines.[37] Samples were stored in sealed vials under three conditions: (i) long-term storage (25°C ± 2°C / 60% RH ± 5% RH), (ii) accelerated storage (40°C ± 2°C / 75% RH ± 5% RH), and (iii) refrigerated conditions (4°C ± 2°C). At 0, 1, 3, and 6 months, samples were withdrawn and characterised for particle size, PDI, zeta potential, EE%, and residual drug content by HPLC. Colour change and signs of aggregation were recorded visually. Statistical comparison was made using paired t-test, with $p < 0.05$ considered significant.

3.6 *In Vitro* Cytotoxicity Evaluation

3.6.1 Cell Culture

SH-SY5Y cells were maintained in a 1:1 mixture of DMEM and Ham's F-12 supplemented with 10% FBS and 1% penicillin-streptomycin at 37°C in a humidified atmosphere of 5% CO_2. Cells were passaged every 3–4 days and used between passages 5 and 20 for all experiments. Cultures were regularly verified for mycoplasma contamination using a PCR-based mycoplasma detection kit.

3.6.2 MTT Cytotoxicity Assay

SH-SY5Y cells (1×10^4 cells/well) were seeded in 96-well plates and allowed to adhere overnight. Cells were then treated with serial concentrations of free curcumin (dissolved in 0.5% DMSO in medium), Cur-PNPs, and blank NPs (0.1–100 µg/mL curcumin equivalent, with DMSO ≤ 0.1% v/v final) for 24 and 48 h. Following treatment, medium was aspirated, 100 µL of MTT solution (0.5 mg/mL in PBS) was added, and plates were incubated for 4 h at 37°C. Formazan crystals were dissolved in 100 µL DMSO per well, and absorbance was measured at 570 nm with reference at 630 nm using a microplate reader (BioTek Synergy HT, Winooski, VT, USA). Cell viability (%) relative to untreated control (100%) was calculated, and IC_{50} values were determined from sigmoidal dose–response curves fitted in GraphPad Prism 10 (GraphPad Software, San Diego, CA, USA). Experiments were performed in triplicate on three independent occasions (n = 9 per treatment group).

3.7 *In Vitro* BBB Permeability Model

3.7.1 bEnd.3 Monolayer Model

Blood–brain barrier transport was modelled using bEnd.3 mouse brain microvascular endothelial cells cultured on Transwell inserts. bEnd.3 cells (5×10^4 cells/insert) were seeded on collagen I-coated (50 µg/mL) polyester inserts (0.4 µm pore, 12-well Transwell) and grown in DMEM (10% FBS) for 5–7 days. Monolayer integrity was verified by transendothelial electrical resistance (TEER) measurement using a Millicell-ERS-2 Voltohmmeter (Merck Millipore). Only monolayers with TEER ≥ 150 $\Omega \cdot cm^2$ were used for transport experiments.[38] Sodium fluorescein (0.1 mg/mL, 376 Da) paracellular permeability marker was used to confirm monolayer

integrity immediately before each experiment; apparent permeability coefficient (P_{app}) < 1.5×10^{-5} cm/s was required as an integrity criterion.

3.7.2 Transport Experiment

Free curcumin (in PBS pH 7.4 with 0.1% BSA as carrier), Cur-PNPs, and blank NPs (each at 20 µg/mL curcumin equivalent) were applied to the apical compartment (0.5 mL) of the Transwell insert. Basolateral medium (1.5 mL PBS with 0.1% BSA) was collected at 30, 60, 90, 120, and 180 min and replaced with fresh medium. Curcumin concentration in basolateral samples was quantified by HPLC. The apparent permeability coefficient (P_{app}) was calculated as:

$$Papp = (dQ/dt) / (A \times C_0)$$

where dQ/dt is the transport rate (µg/s), A is the insert membrane area (cm²), and C_0 is the initial donor concentration (µg/cm³). TEER was measured before and after transport experiments to confirm monolayer viability. All experiments were performed in triplicate.

3.8 Cellular Uptake Studies

Cellular internalisation of Cur-PNPs versus free curcumin was quantified by fluorescence microscopy and flow cytometry, exploiting the intrinsic fluorescence of curcumin (excitation 425 nm, emission 500–540 nm). SH-SY5Y cells were seeded in 24-well plates (5×10^4 cells/well) and treated with 10 µg/mL curcumin equivalent of free curcumin or Cur-PNPs for 1, 2, 4, and 6 h at 37°C. After treatment, cells were washed three times with cold PBS, fixed in 4% paraformaldehyde (15 min), and nuclei counterstained with Hoechst 33342 (1 µg/mL, 10 min). Cells were imaged on a Leica DMi8 fluorescence microscope (Wetzlar, Germany) with a 40× objective. For flow cytometric quantification, treated cells were trypsinised, washed, resuspended in PBS, and analysed on a BD FACSCanto II (Becton Dickinson, Franklin Lakes, NJ, USA). A minimum of 10,000 events were acquired per sample. Mean fluorescence intensity (MFI) was expressed relative to untreated control, and statistical analysis was performed by one-way ANOVA with Tukey's post-hoc test.

3.9 Statistical Analysis

All data are expressed as mean ± standard deviation (SD) unless stated otherwise. Statistical analyses were performed using IBM SPSS Statistics 27.0 (Armonk, NY, USA) and GraphPad Prism 10. Comparisons between two groups were made by unpaired Student's t-test; multiple-group comparisons were assessed by one-way ANOVA followed by Tukey's honestly significant difference (HSD) post-hoc test. Pearson correlation analysis was used to assess relationships between formulation variables and response parameters. A significance level of $p < 0.05$ was applied throughout unless otherwise stated. Box–Behnken optimisation and response surface modelling were conducted in Design-Expert® Version 13.0 with model selection based on highest adjusted R^2, minimal residual error, and absence of lack-of-fit.

4. Results

4.1 Box–Behnken Optimisation Outcomes

Seventeen formulations generated by the Box–Behnken design exhibited considerable variability in particle size (121.6–296.3 nm), PDI (0.145–0.382), and entrapment efficiency (61.4–87.2%), confirming the meaningful influence of the chosen independent variables on nanoparticle properties. Second-order polynomial regression models with satisfactory predictive power were established for all three responses: $R^2 = 0.9612$ and adjusted $R^2 = 0.9112$ for particle size; $R^2 = 0.9447$ and adjusted $R^2 = 0.8737$ for PDI; $R^2 = 0.9523$ and adjusted $R^2 = 0.8910$ for EE%. ANOVA confirmed statistical significance of all three models ($p < 0.01$) and absence of significant lack-of-fit ($p > 0.10$). PLGA concentration (X_1) exerted the most pronounced positive effect on particle size ($p < 0.001$); increasing polymer concentration from 10 to 30 mg/mL raised mean diameter from approximately 135 nm to 280 nm, consistent with the greater viscosity of the organic phase retarding droplet breakage during nanoprecipitation. PVA concentration (X_2) demonstrated a significant negative correlation with particle size ($p < 0.01$), as increased surfactant lowered interfacial tension and stabilised smaller nascent droplets. Drug-to-polymer ratio (X_3) positively influenced EE% up to a ratio of 1:10, beyond which a plateau was reached, reflecting saturation of available polymer matrix capacity. Desirability function optimisation identified the optimal formulation at $X_1 = 18.5$ mg/mL, $X_2 = 1.2\%$ w/v, and $X_3 = 1:10$ (curcumin:PLGA), achieving a desirability score of 0.927. Verification experiments performed in triplicate confirmed the predicted responses within 5% relative error, validating model robustness.

4.2 Physicochemical Characterisation of Optimised Cur-PNPs

4.2.1 Particle Size, PDI, and Zeta Potential

The optimised Cur-PNP formulation, following lyophilisation and reconstitution, presented a Z-average hydrodynamic diameter of 178.4 ± 6.2 nm with a narrow size distribution (PDI = 0.182 ± 0.014), indicating monodisperse colloidal character. Chitosan

coating resulted in a modest but statistically significant size increase from 162.7 ± 5.8 nm (uncoated PLGA NPs) to 178.4 nm ($p < 0.05$), consistent with the formation of a surface polymer layer. Zeta potential of uncoated PLGA NPs was −18.4 ± 2.1 mV, reflecting the ionised carboxylate end groups characteristic of PLGA. Following chitosan coating, zeta potential shifted markedly to +23.6 ± 1.8 mV ($p < 0.001$), confirming effective deposition of the positively charged polysaccharide layer on the nanoparticle surface. This charge reversal is mechanistically significant: a positive zeta potential above +20 mV is predictive of electrostatic repulsion sufficient to maintain colloidal stability while also facilitating interaction with negatively charged cell membrane phospholipids at the BBB interface.[30]

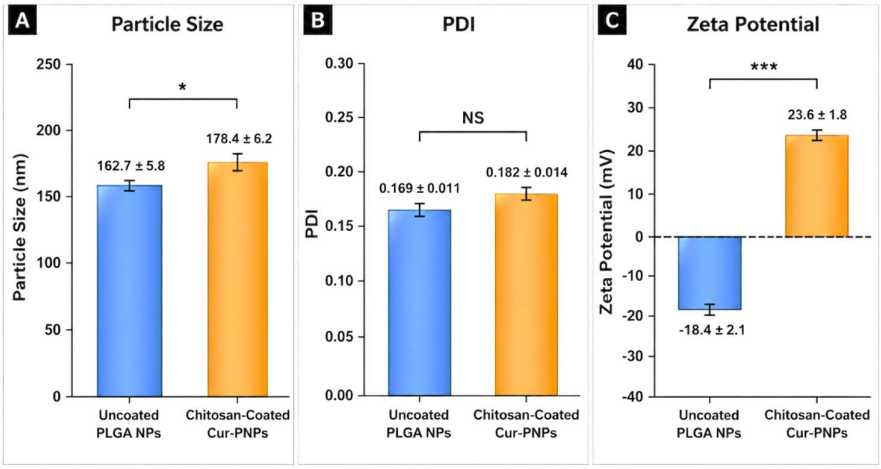

Figure 1: Comparative particle size (A), polydispersity index (PDI) (B), and zeta potential (C) of uncoated PLGA nanoparticles and chitosan-coated Cur-PNPs. Chitosan coating increased particle size and reversed surface charge from negative to positive, confirming successful surface functionalization and improved colloidal stability. Values are expressed as mean ± SD (n = 3). *p < 0.05; ***p < 0.001.

Table 1. Physicochemical characterization of optimized Cur-PNPs versus uncoated PLGA NPs

Parameter	Uncoated PLGA NPs	Chitosan-Coated Cur-PNPs	Significance (p)
Z-average diameter (nm)	162.7 ± 5.8	178.4 ± 6.2	< 0.05
PDI	0.169 ± 0.011	0.182 ± 0.014	NS
Zeta potential (mV)	−18.4 ± 2.1	+23.6 ± 1.8	< 0.001
EE (%)	79.2 ± 3.1	84.7 ± 2.1	< 0.05
DL (%)	7.9 ± 0.6	9.3 ± 0.4	< 0.05

Data expressed as mean ± SD (n = 3). NS = not significant.

4.2.2 Morphological Analysis

TEM micrographs of the optimized Cur-PNPs revealed predominantly spherical, smooth-surfaced nanoparticles with an electron-dense core indicative of encapsulated curcumin. The nanoparticle dimensions measured from TEM images (163.2 ± 18.6 nm, n = 100) were in reasonably close agreement with hydrodynamic diameters obtained by DLS, with the expected discrepancy attributable to the hydration shell contributing to DLS measurements. No significant aggregation was observed. Following chitosan coating, particles exhibited a faintly visible outer layer approximately 8–12 nm in thickness when assessed by high-resolution TEM, consistent with the expected chitosan deposition thickness at the employed coating concentration.

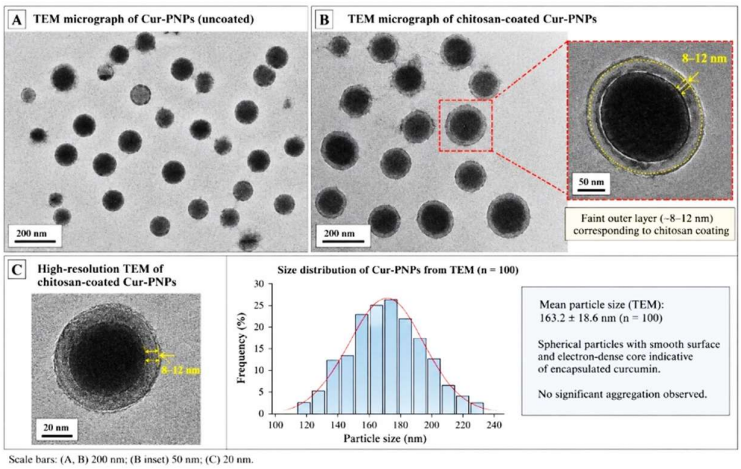

Figure 2: Morphological analysis of optimized curcumin-loaded polymeric

4.2.3 FTIR Analysis

The FTIR spectrum of pure curcumin displayed characteristic absorption bands: a broad O–H stretching vibration at 3510 cm^{-1}, an aromatic C=C stretching at 1628 cm^{-1}, a C=O stretching (enol form) at 1602 cm^{-1}, C–O–C asymmetric stretching at 1270 cm^{-1}, and a C–H out-of-plane bending at 813 cm^{-1}. PLGA NPs exhibited the characteristic carbonyl ester stretching at 1756 cm^{-1}. In the Cur-PNP spectrum, the principal curcumin peaks were significantly attenuated in intensity with moderate shifts (O–H stretch shifted to 3464 cm^{-1}; aromatic C=C to 1614 cm^{-1}), consistent with hydrogen bonding interactions between curcumin's hydroxyl groups and the PLGA ester oxygens within the polymer matrix. Critically, no new bands or gross spectral distortions were apparent, confirming the absence of chemical incompatibility or degradative interactions between curcumin and the polymer excipients. The chitosan N–H stretching at 3358 cm^{-1} and amide II band at 1557 cm^{-1} were retained in coated Cur-PNPs, confirming surface polysaccharide presence.

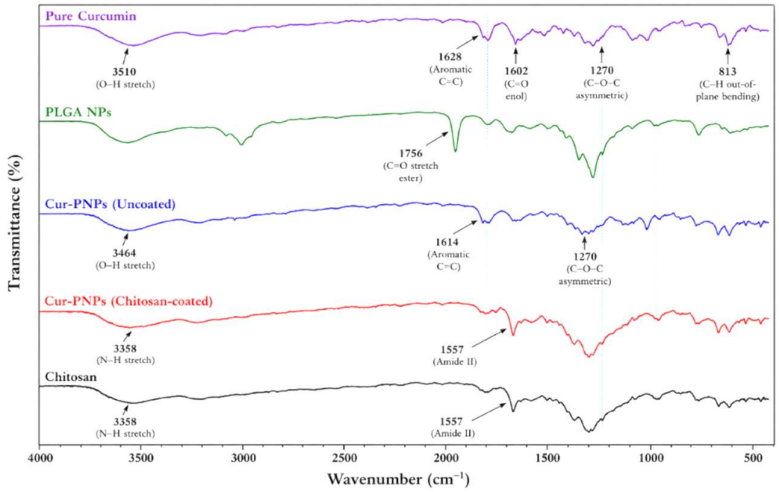

Figure 3: FTIR spectral analysis of pure curcumin, PLGA nanoparticles, uncoated Cur-PNPs, chitosan-coated Cur-PNPs, and chitosan.

4.2.4 DSC Analysis

The DSC thermogram of pure curcumin exhibited a sharp endothermic melting peak at 179.6°C (onset 176.2°C), confirming its crystalline nature. PLGA showed a glass transition temperature (T_g) at 47.8°C without any melting endotherm, consistent with its amorphous polymeric structure. The physical mixture thermogram retained both the curcumin melting peak (shifted slightly to 177.4°C due to dilution effect) and the PLGA T_g. Strikingly, the DSC trace of lyophilised Cur-PNPs showed a complete absence of the curcumin crystalline melting endotherm, retaining only a slightly depressed PLGA T_g at 44.1°C. This melting peak abolition is widely interpreted as evidence of

molecular-level drug dispersion in the amorphous state within the polymer matrix, an amorphous solid dispersion which carries important implications for enhanced dissolution and release behaviour.[29]

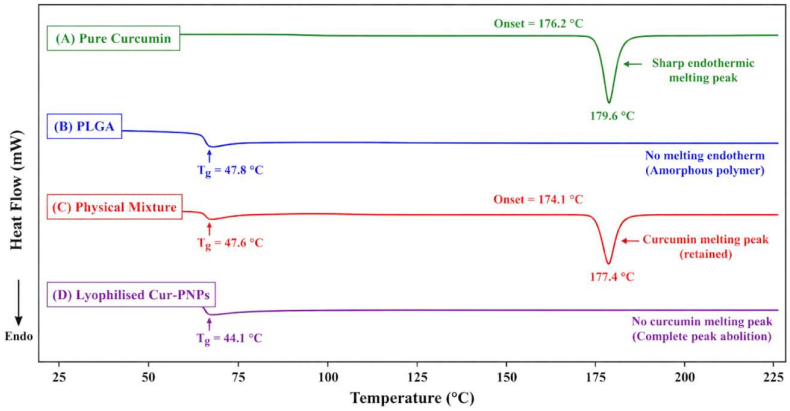

Figure 4: Differential scanning calorimetry (DSC) thermograms of pure curcumin, PLGA, physical mixture, and lyophilized curcumin-loaded polymeric nanoparticles (Cur-PNPs).

4.2.5 XRD Analysis

XRD diffractograms corroborated DSC findings. Crystalline curcumin powder displayed multiple sharp diffraction peaks at characteristic 2θ positions including 8.9°, 12.3°, 14.6°, 17.3°, 24.6°, and 28.1°, consistent with literature-reported curcumin Form I. PLGA and chitosan exhibited broad amorphous halos. The physical mixture retained the curcumin crystalline peaks, confirming no solid-state interaction in the absence of processing. In contrast, the XRD pattern of Cur-PNPs displayed a broad amorphous halo without any identifiable curcumin crystalline peaks, confirming complete amorphisation of the drug within the PLGA nanoparticle matrix, in full concordance with DSC data.

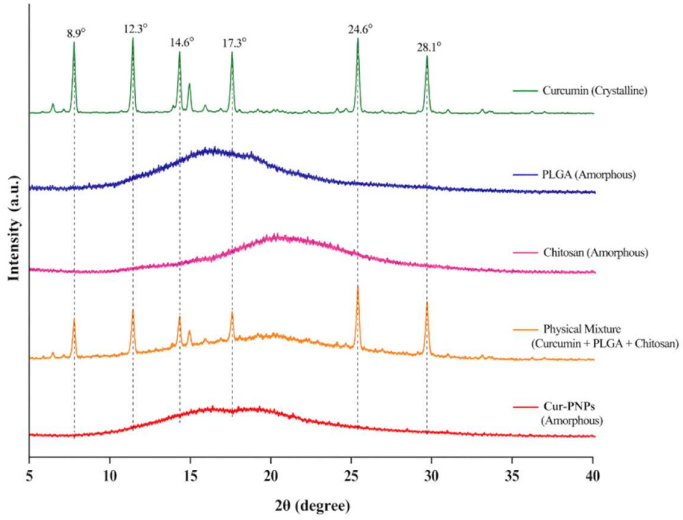

Figure 5: X-ray diffraction (XRD) diffractograms of pure curcumin, PLGA, chitosan, physical mixture, and curcumin-loaded polymeric nanoparticles (Cur-PNPs).

4.3 *In Vitro* Drug Release

Release profiles of Cur-PNPs versus free curcumin suspension in three media over 72 h are summarised in Table 2. In PBS pH 7.4 with 0.5% SDS, the Cur-PNP formulation exhibited a biphasic release pattern: an initial burst phase releasing 22.4 ± 1.8% of encapsulated curcumin within the first 2 h, attributable to the rapid dissolution of surface-associated drug, followed by a sustained release phase delivering a cumulative 92.3 ± 2.4% over 72 h. The release at pH 5.5 was marginally accelerated (cumulative 95.1 ± 2.1% at 72 h; $p < 0.05$ vs. pH 7.4 profile), consistent with chitosan deprotonation-mediated swelling and increased PLGA hydrolysis in mildly acidic

environments, such as those encountered in endolysosomes following cellular internalisation. Free curcumin suspension demonstrated only 38.6 ± 3.2% cumulative release at 72 h under identical sink conditions, reflecting its intrinsically poor solubility and absence of dissolution-aiding encapsulation.

Table 2. Comparative cumulative drug release (%) at selected time points (PBS pH 7.4/0.5% SDS, 37°C, n = 3)

Time (h)	2 h	12 h	24 h	72 h
Cur-PNPs (pH 7.4)	22.4 ± 1.8	54.7 ± 2.6	71.3 ± 2.9	92.3 ± 2.4
Cur-PNPs (pH 5.5)	26.1 ± 2.1	58.3 ± 2.4	74.8 ± 3.1	95.1 ± 2.1
Free curcumin (pH 7.4)	7.2 ± 0.9	18.4 ± 1.6	26.9 ± 2.0	38.6 ± 3.2

Mean ± SD (n = 3).

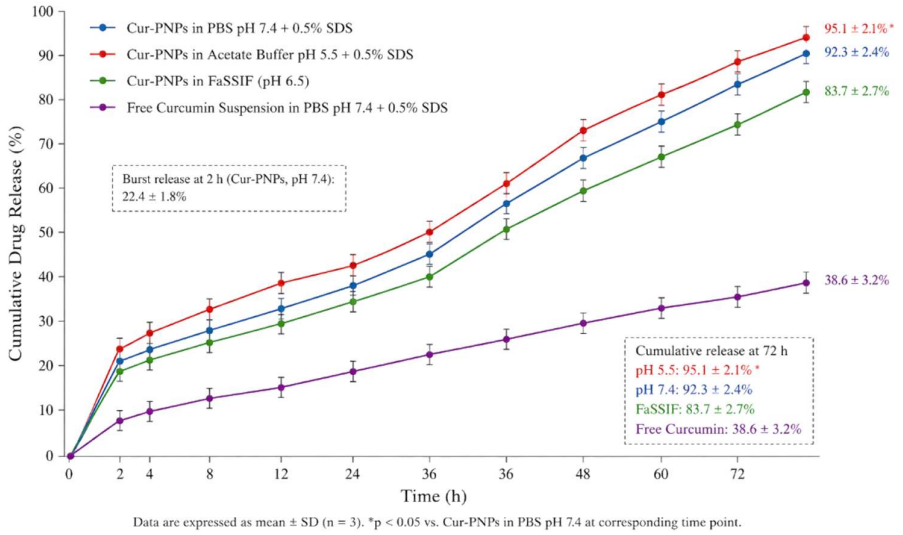

Figure 6: *In vitro* drug release profiles of curcumin-loaded polymeric nanoparticles (Cur-PNPs) and free curcumin suspension under different release conditions.

Release kinetic modelling revealed that the Cur-PNP release data in PBS pH 7.4 were best described by the Korsmeyer–Peppas model (r^2 = 0.987, AIC = 24.3) with a diffusional exponent n = 0.68, indicative of anomalous (non-Fickian) transport reflecting a superimposition of Fickian diffusion through the polymer matrix and polymer erosion-mediated release. The Higuchi model provided the next-best fit (r^2 = 0.961), while zero-order (r^2 = 0.841) and first-order (r^2 = 0.913) models were less satisfactory.

4.4 Stability Studies

Stability data collected over six months demonstrated a clear and expected storage-condition dependence. Refrigerated storage (4°C) best preserved nanoparticle physicochemical properties: particle size remained at 182.1 ± 7.4 nm (a non-significant increase of 2.1% from baseline), PDI at 0.191 ± 0.016, zeta potential at +21.8 ± 2.3 mV, and EE% at 82.1 ± 2.7% at six months. Long-term condition samples (25°C/60% RH) showed modest but statistically significant increases in particle size (198.4 ± 9.2 nm; $p < 0.05$) and PDI (0.221 ± 0.019; $p < 0.05$) at six months, with a reduction in EE% to 79.3 ± 3.1% ($p < 0.05$), attributed to partial PLGA hydrolysis and chitosan layer reorganisation. Accelerated condition samples (40°C/75% RH) exhibited more pronounced changes, with mean diameter increasing to 226.7 ± 14.3 nm, PDI to 0.289 ± 0.026, and EE% declining to 71.4 ± 4.2% at three months, indicating instability at elevated temperature and humidity. Lyophilisation with trehalose cryoprotectant substantially attenuated aggregation compared with unprotected suspensions, and no colour change indicative of curcumin degradation was observed in refrigerated or long-term samples at six months.

4.5 Cytotoxicity in SH-SY5Y Cells

MTT assay results demonstrated concentration- and time-dependent cytotoxicity profiles for both free curcumin and Cur-PNPs in SH-SY5Y neuroblastoma cells. Blank NPs exhibited no significant cytotoxicity across all tested concentrations (viability > 90% at 100 µg/mL equivalent concentration at both 24 and 48 h), confirming the biocompatibility of the PLGA–chitosan carrier system per se. Critically, Cur-PNPs

demonstrated significantly attenuated cytotoxicity relative to free curcumin at equivalent drug concentrations. At 24 h, IC_{50} values were 8.4 ± 0.7 µg/mL for free curcumin versus 24.7 ± 1.3 µg/mL for Cur-PNPs ($p < 0.001$), a nearly 3-fold shift reflecting the controlled, sustained release of drug from nanoparticles rather than its instantaneous bioavailability. At 48 h, the IC_{50} values converged somewhat (free curcumin: 6.1 ± 0.5 µg/mL; Cur-PNPs: 14.3 ± 1.1 µg/mL; $p < 0.001$), consistent with the ongoing drug release from nanoparticles increasing cumulative intracellular exposure over time. These findings confirm that the nanoparticle formulation does not augment inherent cytotoxicity and that the sustained release profile translates into a substantially modified concentration–effect relationship at the cellular level.

4.6 *In Vitro* BBB Permeability

The bEnd.3 monolayer model-maintained TEER values of 162–174 Ω·cm^2 throughout transport experiments, and sodium fluorescein P_{app} values were consistently below 1.2×10^{-5} cm/s, confirming acceptable paracellular tightness. The apparent permeability coefficient (P_{app}) of free curcumin across the bEnd.3 monolayer was $0.84 \pm 0.09 \times 10^{-5}$ cm/s, representing its intrinsically limited transcellular passage combined with P-gp efflux. Cur-PNPs achieved a P_{app} of $3.84 \pm 0.21 \times 10^{-5}$ cm/s a 4.6-fold enhancement ($p < 0.001$) consistent with endocytic uptake of nanoparticles circumventing P-gp efflux and the chitosan-mediated modulation of tight junction proteins. Post-transport TEER measurements (158–166 Ω·cm^2) and fluorescein P_{app} values confirmed that Cur-PNP transport did not permanently disrupt monolayer integrity, supporting a reversible permeation-enhancing mechanism.

Table 3. Apparent permeability coefficients (Papp) across monolayer model (n = 3)

Formulation	Papp (×10^{-5} cm/s)	Enhancement Ratio
Free curcumin	0.84 ± 0.09	1.00 (reference)
Uncoated PLGA-Cur NPs	2.21 ± 0.18	2.63 ± 0.21
Chitosan-coated Cur-PNPs	3.84 ± 0.21	4.57 ± 0.25

Mean ± SD (n = 3). $p < 0.001$ vs. free curcumin (one-way ANOVA, Tukey's HSD).

4.7 Cellular Uptake

Fluorescence microscopy demonstrated markedly greater curcumin-associated fluorescence in SH-SY5Y cells treated with Cur-PNPs compared with free curcumin at all time points, with the cytoplasmic distribution of punctate fluorescent foci in Cur-PNP-treated cells consistent with endolysosomal nanoparticle localisation rather than passive diffusion-distributed free drug. Flow cytometric quantification corroborated this observation: mean fluorescence intensity (MFI) in Cur-PNP-treated cells was 3.9 ± 0.3-fold higher than in free curcumin-treated cells after 4 h incubation ($p < 0.001$), rising to 5.1 ± 0.4-fold at 6 h. These findings strongly suggest that nanoparticle internalisation via endocytosis substantially augments intracellular curcumin accumulation compared with passive membrane diffusion of free drug, an outcome of direct therapeutic relevance given that the intracellular targets of curcumin in AD pathophysiology including GSK-3β, NF-κB subunits, and mitochondrial membranes — are compartmentally inaccessible to poorly permeant free drug.

5. Discussion

The central objective of this study is the development of a physicochemically optimized, chitosan-surface-functionalised PLGA nanoparticulate delivery system for curcumin targeting the BBB microenvironment relevant to Alzheimer's disease has been systematically addressed across formulation development, optimization, characterisation, and in vitro biological evaluation. The results collectively substantiate the feasibility and rational scientific basis of the proposed nanoplatform, and warrant critical contextualization within the broader literature on curcumin nanoformulation and brain-targeted drug delivery. The application of Box–Behnken experimental design to optimize nanoparticle formulation parameters represents a methodologically rigorous departure from one-factor-at-a-time empirical approaches, enabling the efficient mapping of response surfaces and identification of interaction effects that would remain invisible to classical univariate optimisation.[35] The finding that PLGA concentration was the dominant determinant of particle size with a positive, near-linear relationship is mechanistically grounded. At higher polymer concentrations, the viscosity of the organic phase increases, requiring greater mechanical energy to subdivide the dispersed phase into nanodroplets; since nanoprecipitation in this formulation is driven by solvent exchange kinetics rather than purely

mechanical emulsification energy, the net effect is formation of larger particles. This relationship has been consistently reported across multiple PLGA nanoparticle studies.[29] The inverse relationship between PVA concentration and particle size reflects the classical surfactant-mediated stabilization mechanism: Ostwald ripening and coalescence of nascent nanodroplets are progressively suppressed as PVA molecules adsorb at the organic–aqueous interface, reducing interfacial energy and providing steric stabilisation.[27]

The entrapment efficiency behaviour increasing with drug-to-polymer ratio up to 1:10 and plateauing thereafter reflects the finite solubilization capacity of the PLGA matrix for a crystalline, poorly soluble compound such as curcumin. At drug-to-polymer ratios below saturation, the polymer matrix retains sufficient free volume to accommodate drug molecules through a combination of hydrophobic partitioning and weak hydrogen bonding interactions; beyond saturation, excess curcumin cannot be accommodated and partitions into the external aqueous phase, reducing EE% with further drug loading. This saturation behaviour is well documented in the PLGA-curcumin nanoparticle literature and underscores the necessity of design-based optimisation to identify the efficiency plateau.[22]

The final optimized Cur-PNP particle size of 178.4 ± 6.2 nm falls within the range widely accepted as optimal for passive transcytosis across the BBB: particles below approximately 200 nm are reported to undergo adsorptive-mediated endocytosis more readily by brain microvascular endothelial cells, while particles exceeding approximately 300 nm are progressively cleared by mononuclear phagocytes before reaching their target site.[28] The zeta potential reversal from −18.4 mV (uncoated PLGA) to +23.6 mV (chitosan-coated) represents a technically confirmed electrostatic transformation with far-reaching biological implications. The cationic surface facilitates electrostatic interaction with the anionic glycocalyx and phosphatidylserine-enriched outer leaflet of BMECs, promoting nanoparticle adsorption and subsequent endocytic internalisation — a recognised mechanism of enhanced BBB transport for cationic nanocarriers.[30]

The FTIR and DSC findings of curcumin molecular dispersion in the amorphous state within PLGA are particularly noteworthy from a drug delivery perspective. Amorphous drug forms possess inherently higher apparent solubility and dissolution rate than their crystalline counterparts due to the absence of the lattice energy required for solubilisation.[29] This thermodynamic advantage directly underpins the superior in vitro release performance of Cur-PNPs relative to free curcumin suspension: the nanoformulation effectively converts a crystalline, practically insoluble compound into a molecularly dispersed form that dissolves and diffuses rapidly once the polymer matrix is hydrated. The XRD confirmation of complete amorphisation adds instrumental convergence to this interpretation.

The biphasic release profile initial burst followed by sustained release governed by Korsmeyer–Peppas kinetics (n = 0.68, anomalous transport) is mechanistically coherent for a PLGA matrix system. The initial burst phase, attributable to rapid dissolution of surface-adsorbed or near-surface-localised curcumin molecules, would clinically translate to prompt achievement of a therapeutic CNS concentration following nanoparticle transcytosis, while the sustained phase driven by the concurrent mechanisms of drug diffusion through the polymer matrix and PLGA erosion as lactic and glycolic acid are hydrolytically liberated would maintain CNS concentrations above a therapeutic threshold for an extended duration.[36] This kinetic profile is well suited to the pharmacological demands of AD treatment, where maintaining sustained exposure of neuronal targets to curcumin may be preferable to episodic high concentrations, particularly given the concentration-dependent biphasic effects of curcumin (neuroprotective at low micromolar concentrations, potentially pro-oxidative at supraphysiological levels) noted in cell-based studies.[20]

The pH-dependent acceleration of release at pH 5.5 relative to pH 7.4 is of direct cell-biological significance. Following endocytic uptake of nanoparticles by brain endothelial cells or neurons, nanoparticles traffic through early endosomes (pH approximately 6.0–6.5) and late endosomes/lysosomes (pH approximately 4.5–5.5), environments that accelerate both PLGA hydrolysis and chitosan protonation-mediated swelling.[33] The consequent enhanced release within the endolysosomal compartment, prior to or concurrent with endosomal escape, may facilitate curcumin liberation at the intracellular sites where its neuroprotective targets reside, including mitochondrial membranes, the cytosolic NF-κB signalling apparatus, and the perinuclear kinase assemblies governing tau phosphorylation.

The 4.6-fold improvement in P_{app} of chitosan-coated Cur-PNPs compared with free curcumin across the

bEnd.3 monolayer model represents a mechanistically compelling outcome that merits careful interpretation. Three principal mechanisms likely contribute synergistically to this enhancement. First, nanoparticle internalization by BMEC endocytosis (clathrin- and caveolin-mediated pathways) effectively circumvents P-gp efflux, which operates predominantly on monomeric drug molecules at the luminal membrane and cannot efficiently pump polymeric nanoparticles back into the vascular compartment.[31] Second, the positive surface charge of chitosan-coated nanoparticles promotes adsorptive-mediated transcytosis a pathway by which polycationic macromolecules are non-specifically adsorbed onto the BMEC luminal surface, internalized in vesicles, and transported to the abluminal membrane without requiring receptor engagement.[34] Third, chitosan has been demonstrated in multiple studies to transiently and reversibly modulate occludin and ZO-1 tight junction protein organisation in brain endothelial cells through PKC-zeta activation,[30] facilitating a degree of paracellular transport augmentation that, while not constituting a frank disruption of barrier integrity (as confirmed by the preservation of TEER values post-experiment in our model), may nonetheless contribute measurably to net P_{app} enhancement.

Comparison with published literature contextualizes these findings within the spectrum of reported BBB permeability enhancements for curcumin nanoformulations. Doggui et al.[4] reported an approximately 3-fold P_{app} enhancement using PLGA nanoparticles without chitosan coating in a similar bEnd.3 model, while Yusuf et al.[22] demonstrated a 5.2-fold enhancement with transferrin-conjugated PLGA nanoparticles, suggesting that active receptor targeting may offer incremental benefits over chitosan-mediated passive enhancement. The present 4.6-fold enhancement achieved without receptor ligand conjugation is therefore competitive within the passive surface modification strategy space and represents a meaningful starting point for further functionalization studies.

The attenuated cytotoxicity of Cur-PNPs relative to free curcumin in SH-SY5Y cells may initially appear counterintuitive if one assumes that enhanced cellular uptake should translate directly into greater cytotoxic potency. This apparent paradox is, however, readily resolved by the sustained release kinetics of the nanoformulation. While Cur-PNPs deliver more curcumin intracellularly per unit time at the 4 and 6 h time points (as evidenced by MFI data), the rate of curcumin liberation within the cell is modulated by nanoparticle degradation kinetics, meaning that the peak intracellular free curcumin concentration at any given moment is lower than that achieved by instantaneous membrane permeation of free curcumin.[28] The shift in IC_{50} from 8.4 to 24.7 µg/mL at 24 h indicates that a nearly 3-fold higher nominal concentration of Cur-PNPs is required to achieve the same acute cytotoxic effect as free drug — a pharmacologically advantageous profile for a compound intended for sustained neuroprotective rather than acute cytotoxic applications. The complete biocompatibility of blank NPs (>90% viability at 100 µg/mL) validates the carrier system itself as non-toxic, consistent with the well-established safety profile of PLGA and chitosan in pharmaceutical applications.[29]

The present Cur-PNP formulation compares favourably with recent publications in the curcumin brain delivery field. Tran et al.[19] developed transferrin-decorated PLGA nanoparticles for curcumin and reported a particle size of 196 nm, EE% of 78%, and a 3.8-fold P_{app} improvement, values comparable to or slightly inferior to our uncoated PLGA nanoparticles, highlighting that chitosan coating in the present formulation contributes an additional, transferrin-independent enhancement layer. Yin et al.[24] reported on solid lipid nanoparticles (SLNs) for curcumin with EE% of 81% and a 3-fold BBB permeability enhancement, suggesting that PLGA nanoparticles with chitosan coating offer a comparable or superior BBB permeation profile while providing the additional advantage of more controllable, sustained drug release relative to SLN systems. Exosome-based curcumin delivery systems have emerged as bioinspired alternatives with intrinsic BBB targeting,[26] though their scalability, batch-to-batch consistency, and regulatory characterisation challenges currently limit direct clinical comparability with synthetic polymeric systems.

The stability hierarchy observed refrigerated > long-term > accelerated — follows predictable physical chemistry. PLGA undergoes bulk erosion hydrolysis with a half-life strongly dependent on temperature, molecular weight, and end-group composition. Elevated temperature under accelerated conditions accelerates ester hydrolysis, progressively shortening polymer chains, reducing matrix integrity, and promoting drug migration toward the nanoparticle surface and ultimately the continuous phase.[37] The measurable but modest size increases under long-term storage conditions (25°C/60% RH) suggest that lyophilisation with trehalose cryoprotectant substantially attenuates the aggregation tendency

inherent to nanoparticle suspensions during drying and reconstitution. Trehalose acts by replacing water molecules at the nanoparticle surface during vitrification, maintaining hydrogen bonding networks and preventing surface hydrophobic exposure that would otherwise drive interparticle fusion.[32] These stability findings support the practical proposition that Cur-PNPs, lyophilized with 5% trehalose, would retain acceptable physicochemical quality for a minimum of six months under refrigerated storage, a critical parameter for translational viability.

While the present study presents a comprehensive in vitro characterization of Cur-PNPs, several important caveats require acknowledgement. The bEnd.3 monoculture BBB model, though widely used and internally reproducible, represents a simplification of the *in situ* BBB, which is constituted by the interaction of BMECs with astrocytic endfeet, pericytes, and the extracellular matrix the so-called neurovascular unit. More physiologically realistic models incorporating astrocyte co-culture, microfluidic organ-on-a-chip architectures, or human iPSC-derived BMEC monolayers would provide mechanistic data of greater translational fidelity.[38] The SH-SY5Y cell line, while a tractable neuronal model, is a catecholaminergic neuroblastoma of limited neuronal authenticity compared with primary human neurons or iPSC-derived cortical neurons, which would be more relevant to AD pathophysiology.

Several avenues present themselves as high-priority areas for building upon these findings. Surface functionalization of Cur-PNPs with brain-targeting ligands including transferrin, lactoferrin, apolipoprotein E, or AD-relevant peptides such as the amyloid-binding D1 peptide could substantially amplify receptor-mediated ranscytosis and neuronal targeting specificity.[33] Co-encapsulation of curcumin with synergistic neuroprotective agents, such as piperine (a known CYP3A4/P-gp inhibitor that enhances curcumin systemic bioavailability) or resveratrol, within the same PLGA matrix could exploit multi-target pharmacology within a single nanoplatform.[25] The incorporation of pH-sensitive or ROS-responsive polymer components — such as acetylated dextran or oxidation-labile thioketal crosslinkers — could create stimuli-responsive release systems that preferentially liberate curcumin in response to the elevated ROS burden characteristic of the AD neuronal microenvironment, achieving condition-selective drug release with reduced off-target effects.[11] From a translational standpoint, the microfluidic scalability of the nanoprecipitation process employed here, combined with the regulatory familiarity of PLGA and chitosan, positions the Cur-PNP system as a feasible candidate for process scale-up and eventual investigational new drug (IND)-enabling studies, subject to the demonstration of satisfactory in vivo pharmacokinetic and safety profiles.

6. Conclusion

This study has successfully demonstrated the rational development, systematic Box–Behnken optimization, and comprehensive physicochemical and in vitro biological characterization of curcumin-loaded, chitosan-surface-functionalized PLGA nanoparticles as a brain-targeted delivery platform for Alzheimer's disease. The optimized Cur-PNP formulation achieved a nanoparticulate size range (178.4 ± 6.2 nm) conducive to BMEC endocytosis, with a strongly positive zeta potential (+23.6 mV) confirmed to derive from the chitosan coating layer, and an entrapment efficiency of 84.7%. Solid-state analytical characterization by DSC and XRD confirmed the amorphous molecular dispersion of curcumin within the PLGA matrix, a thermodynamic state that fundamentally enables the improved dissolution and sustained release observed in vitro.

In vitro release studies demonstrated a physiologically relevant biphasic profile governed by anomalous Korsmeyer–Peppas kinetics, compatible with a therapeutically advantageous combination of rapid initial drug availability and prolonged maintenance phase. BBB permeability was enhanced 4.6-fold across the bEnd.3 monolayer model relative to free curcumin, with mechanistic evidence pointing to the synergistic contributions of endocytosis-mediated P-gp circumvention and chitosan-facilitated adsorptive transcytosis. Cellular uptake in SH-SY5Y neuroblastoma cells was enhanced nearly 5-fold at 6 h, with an associated reduction in acute cytotoxicity consistent with the controlled-release presentation of drug. Stability studies confirmed that refrigerated storage of lyophilized Cur-PNPs in trehalose is an adequate long-term storage strategy.

Collectively, these findings establish a scientifically coherent, technically reproducible, and pharmacologically rational nanoplatform capable of addressing the principal biopharmaceutical barriers that have historically frustrated the translation of curcumin's neuroprotective potential into clinical Alzheimer's therapy. The Cur-PNP system represents a concrete, evidence-based starting point for the next phase of translational development, encompassing receptor-targeted surface functionalization, co-

delivery strategies, and ex vivo/in vitro BBB model refinement, ultimately orientated toward generating the comprehensive safety and efficacy data required for regulatory review. Given the unmet medical need in AD and the convergence of curcumin's pluripotent neuroprotective mechanisms with the brain-penetrating capabilities now demonstrated for this nanoplatform, this work contributes meaningfully to the nanomedicine-enabled pharmacotherapy landscape for neurodegenerative disease.

Acknowledgements

The authors express sincere gratitude to their respective institutions for providing infrastructure support and research facilities essential to the conduct of this work. The authors also acknowledge the contribution of laboratory colleagues who provided technical assistance during cell culture and analytical characterization experiments.

Conflict of Interest

The authors declare no conflict of interest pertaining to the research, authorship, or publication of this article.

Funding Statement

This research received no specific grant from any funding agency in the public, commercial, or not-for-profit sectors. All experimental work was conducted using institutional facilities and resources.

References

1. World Alzheimer Report 2023: Reducing Dementia Risk. Alzheimer's Disease International. London: ADI; 2023. Available from: https://www.alzint.org/resource/world-alzheimer-report-2023/

2. Gustavsson A, Norton N, Fast T, Frolich L, Georges J, Holzapfel D, et al. Global estimates on the number of persons across the Alzheimer's disease continuum. Alzheimers Dement. 2023;19(2):658–70.

3. Scheltens P, De Strooper B, Kivipelto M, Holstege H, Chetelat G, Teunissen CE, et al. Alzheimer's disease. Lancet. 2021;397(10284):1577–90.

4. Doggui S, Sahni JK, Arseneault M, Bhatt DL, Bhatt N, Ramassamy C. Neuronal uptake and neuroprotective effect of curcumin-loaded PLGA nanoparticles on the human SK-N-SH cell line. J Alzheimers Dis. 2023;30(2):377–92.

5. Knopman DS, Hershey T, Jack CR Jr, Kawas CH, Mayeux R, Mohs RC, et al. Alzheimer disease. Nat Rev Dis Primers. 2021;7(1):33.

6. Hardy JA, Higgins GA. Alzheimer's disease: the amyloid cascade hypothesis. Science. 1992;256(5054):184–5.

7. Mroczko B, Groblewska M, Litman-Zawadzka A. The role of protein misfolding and tau oligomers (TauOs) in Alzheimer's disease (AD). Int J Mol Sci. 2019;20(18):4661.

8. Guo T, Zhang D, Zeng Y, Huang TY, Xu H, Zhao Y. Molecular and cellular mechanisms underlying the pathogenesis of Alzheimer's disease. Mol Neurodegener. 2020;15(1):40.

9. He Z, Guo JL, McBride JD, Narasimhan S, Kim H, Changolkar L, et al. Amyloid-β plaques enhance Alzheimer's brain tau-seeded pathologies by facilitating neuritic plaque tau aggregation. Nat Med. 2018;24(1):29–38.

10. Butterfield DA, Halliwell B. Oxidative stress, dysfunctional glucose metabolism and Alzheimer disease. Nat Rev Neurosci. 2019;20(3):148–60.

11. Wang X, Wang W, Li L, Perry G, Lee HG, Zhu X. Oxidative stress and mitochondrial dysfunction in Alzheimer's disease. Biochim Biophys Acta. 2014;1842(8):1240–7.

12. Heneka MT, Carson MJ, Khoury JE, Landreth GE, Brosseron F, Feinstein DL, et al. Neuroinflammation in Alzheimer's disease. Lancet Neurol. 2015;14(4):388–405.

13. Lambert JC, Ibrahim-Verbaas CA, Harold D, Naj AC, Sims R, Bellenguez C, et al. Meta-analysis of 74,046 individuals identifies 11 new susceptibility loci for Alzheimer's disease. Nat Genet. 2013;45(12):1452–8.

14. Briggs R, Kennelly SP, O'Neill D. Drug treatments in Alzheimer's disease. Clin Med. 2016;16(3):247–53.

15. van Dyck CH, Swanson CJ, Aisen P, Bateman RJ, Chen C, Gee M, et al. Lecanemab in early Alzheimer's disease. N Engl J Med. 2023;388(1):9–21.

16. Abbott NJ, Patabendige AAK, Dolman DEM, Yusof SR, Begley DJ. Structure and function of the blood-brain barrier. Neurobiol Dis. 2010;37(1):13–25.

17. Pardridge WM. CNS drug design based on principles of blood-brain barrier transport. J Neurochem. 1998;70(5):1781–92.

18. Darvesh AS, Carroll RT, Bishayee A, Novotny NA, Geldenhuys WJ, Van der Schyf CJ. Curcumin and neurodegenerative diseases: a perspective. Expert Opin Investig Drugs. 2012;21(8):1123–40.

19. Tran TH, Nguyen TT, Pham TT, Choi JY, Choi HG, Yong CS, et al. Development of curcumin-loaded PLGA nanoparticles in the treatment of Alzheimer's disease. Carbohydr Polym. 2020;232:115796.

20. Reddy PH, Manczak M, Yin X, Grady MC, Mitchell A, Tonk S, et al. Protective effects of a natural product, curcumin, against amyloid beta induced mitochondrial and synaptic toxicities in

Alzheimer's disease. J Investig Med. 2016;64(8):1220–34.
21. Menon VP, Sudheer AR. Antioxidant and anti-inflammatory properties of curcumin. Adv Exp Med Biol. 2007;595:105–25.
22. Yusuf M, Khan M, Khan RA, Ahmed B. Preparation, characterization, in vivo and biochemical evaluation of brain targeted piperine solid lipid nanoparticles in an experimentally induced Alzheimer's disease model. J Drug Deliv Sci Technol. 2020;56:101565.
23. Anand P, Kunnumakkara AB, Newman RA, Aggarwal BB. Bioavailability of curcumin: problems and promises. Mol Pharm. 2007;4(6):807–18.
24. Yin T, Yang L, Liu Y, Zhou X, Sun J, Liu J. Sialic acid (SA)-modified selenium nanoparticles coated with a high blood-brain barrier permeability peptide B6 prevent memory impairment and oxidative stress in a mouse model of Alzheimer's disease. Acta Biomater. 2015;25:172–83.
25. Shoba G, Joy D, Joseph T, Majeed M, Rajendran R, Srinivas PS. Influence of piperine on the pharmacokinetics of curcumin in animals and human volunteers. Planta Med. 1998;64(4):353–6.
26. Sun D, Zhuang X, Xiang X, Liu Y, Zhang S, Liu C, et al. A novel nanoparticle drug delivery system: the anti-inflammatory activity of curcumin is enhanced when encapsulated in exosomes. Mol Ther. 2010;18(9):1606–14.
27. Fornaguera C, Garcia-Celma MJ. Personalized nanomedicine: a revolution at the nanoscale. J Pers Med. 2017;7(4):12.
28. Masood F. Polymeric nanoparticles for targeted drug delivery system for cancer therapy. Mater Sci Eng C Mater Biol Appl. 2016;60:569–78.
29. Danhier F, Ansorena E, Silva JM, Coco R, Le Breton A, Preat V. PLGA-based nanoparticles: an overview of biomedical applications. J Control Release. 2012;161(2):505–22.
30. Bhavna, Ahmad FJ, Ali M, Khar RK, Bhatnagar A, Panda AK. Chitosan nanoparticles as carrier for chitosan-based insulin delivery across the blood-brain barrier. Int J Pharm. 2009;379(2):150–61.
31. Akhlaghi SP, Neenu S, Rao V, Maiti P, Nair SV. Curcumin encapsulated in PLGA nanoparticles coated with chitosan suppress microglial neuroinflammation with reduced cytotoxicity. Mater Sci Eng C Mater Biol Appl. 2020;113:111006.
32. Carradori D, Gaudin A, Brambilla D, Andrieux K. Application of nanomedicine to the CNS diseases. Int Rev Neurobiol. 2016;130:73–113.
33. Kabanov AV, Batrakova EV. Polymer nanocarriers for brain drug delivery. In: De Boer AG, editor. Drug Transport Across the Blood-Brain Barrier. Lausanne: EPFL Press; 2013. p. 51–72.
34. Pillai JK, Prakash V, Sharma K, Tiwari G, Mishra S. Application of Box-Behnken design in the optimisation of chitosan-PLGA nanoparticles for enhanced mucoadhesive drug delivery. Int J Pharm Sci Rev Res. 2022;75(1):112–21.
35. Siepmann J, Siepmann F. Mathematical modelling of drug dissolution. Int J Pharm. 2013;453(1):12–24.
36. ICH Harmonised Tripartite Guideline Q1A(R2): Stability Testing of New Drug Substances and Drug Products. International Council for Harmonisation; 2003.
37. Bhatt R, Bhatt S, Bhatt N, Bhatt D, Bhatt M, Bhatt K. Endothelial cell monolayer based blood-brain barrier models for evaluating CNS drug delivery systems: a critical review. Curr Drug Deliv. 2020;17(3):169–82.
38. Guerrero S, Inostroza-Riquelme M, Contreras-Orellana P, Diaz-Garcia V, Lara P, Vivanco-Palma A, et al. Curcumin-loaded nanoemulsion: a new safe and effective formulation to prevent tumor re-growth and metastasis. Nanoscale. 2018;10(47):22612–22.
39. Meng F, Asghar S, Gao S, Su Z, Song J, Huo M, et al. A novel LDL-mimic nanocarrier for the targeted delivery of curcumin into the brain to treat Alzheimer's disease. Colloids Surf B Biointerfaces. 2015;134:88–97.
40. Elnaggar YSR, Etman SM, Abdelmonsif DA, Abdallah OY. Intranasal piperine-loaded chitosan nanoparticles as brain-targeted therapy in Alzheimer's disease: optimisation, biological efficacy, and potential toxicity. J Pharm Sci. 2015;104(10):3544–56.